Composites: Part A 94 (2017) 113–123

Contents lists available at ScienceDirect

Composites: Part A

journal homepage: www.elsevier.com/locate/compositesa

A viscoelastic approach for modeling bending behavior in finite element forming simulation of continuously fiber reinforced composites

Dominik Dörr [a,*], Fabian J. Schirmaier [a], Frank Henning [a,b], Luise Kärger [a]

[a] Karlsruhe Insititute of Technology (KIT), Institute of Vehicle System Technology (FAST), Department of Lightweight Technology (LBT), Karlsruhe, Germany
[b] Fraunhofer - Institute of Chemical Technology (ICT), Pfinztal, Germany

ARTICLE INFO

Article history:
Received 30 September 2016
Received in revised form 24 November 2016
Accepted 25 November 2016
Available online 27 November 2016

Keywords:
Forming
Process simulation
Finite element analysis (FEA)
Thermoplastic resin

ABSTRACT

An approach for modeling rate-dependent bending behavior in FE forming simulation for either a unidirectional or a woven/bidirectional reinforcement is presented. The applicability of the bending model to both fiber architectures is guaranteed by introducing either an orthogonal or a non-orthogonal fiber parallel material frame. The applied constitutive laws are based on a Voigt-Kelvin and a generalized Maxwell approach. The bending modeling approaches are parameterized according to the characterization of thermoplastic UD-Tape (PA6-CF), where only the generalized Maxwell approach is capable to describe the material characteristic for all of the considered bending rates. A numerical study using a hemisphere test reveals that the Voigt-Kelvin approach and the generalized Maxwell approach lead to similar results for the prediction of wrinkling behavior. Finally, the approaches for modeling bending behavior are applied to a more complex generic geometry as an application test with a good agreement between forming simulation and experimental tests.

1. Introduction

Forming of two-dimensional pre-products into complexly shaped geometries is one of the most determining process steps in manufacturing of continuously fiber-reinforced composites. Thermoforming of thermoplastic pre-impregnated tapes play an increasingly import role and is currently of great interest especially for the automotive industry due to low cycle times and recycleability [1,2].

During forming, several parameters are influencing the forming process of composites, like temperature, blank holders or grippers, fiber orientation or material behavior. Dependent on these material parameters and process conditions, manufacturing defects like wrinkling, gapping or fiber fracture are feasible [3–6]. Furthermore, a change in fiber orientation and fiber volume content, which has a large impact on structural behavior, is inevitable during forming.

Forming simulation enables an initial validation of the process and the determination of suitable process parameters. This can prevent a time consuming and expensive "trial and error" process design. Furthermore, the fiber reorientation due to forming is predictable, which can be used as input value for structural analyses as well as molding analyses to gain good predictions.

Therefore, constitutive modeling approaches offer the possibility of a detailed analysis of the deformation behavior of engineering textiles or preimpregnated blanks during forming, considering material behavior and process conditions. For this purpose, Finite Element Method (FEM) is highly suitable, as the final shape, as well as the stress and strain distribution can be predicted due to the constitutive modeling of the relevant deformation mechanisms. Namely, relevant deformation mechanisms are the intra-ply mechanisms within a single ply and the interface mechanisms between the plies of the stacked laminate. To model these deformation mechanisms, several codes have been developed in the past ten years. In relation to the current interest on composite forming, some commercial codes are available. Particularly, these are the Pam-Form™ code [7], which is based on an explicit approach, and the AniForm™ code [8], which is based on an implicit approach. Furthermore, several models for composite forming simulation with a clear focus on membrane behavior of a single ply are presented in recent publications, where bending behavior is neglected [9–12]. However, as outlined in numerical studies by several authors [13–15], bending behavior has a distinct influence on the prediction of wrinkles during forming. This is also valid, if blankholders or grippers are employed in the forming process [14], which are used to induce membrane forces during forming.

In general, bending behavior is modeled decoupled from membrane behavior, as bending rigidity is very low compared to fiber

* Corresponding author.
E-mail address: dominik.p.doerr@kit.edu (D. Dörr).

http://dx.doi.org/10.1016/j.compositesa.2016.11.027
1359-835X/

stiffness, and thus conventional plate theory is no longer applicable [8,13–18]. Some models are presented in literature, where bending behavior is modeled in a decoupled fashion purely elastic [8,13,15,17] or elastic and temperature-dependent [16,18]. The AniForm™ code offers the possibility of modeling a Voigt-Kelvin approach for the bending behavior, but no details or application of this modeling approach are available in literature. However, as shown by Sachs [19] and Ropers et al. [20], bending behavior of thermoplastic preimpregnated tapes shows a significant rate-dependency at process conditions.

In this work, a finite strain viscoelastic approach for modeling rate-dependent bending behavior using conventional shell elements is presented in the first part. The presented approach is applicable to uni-directional and bi-directional/woven reinforcements by introducing either an orthogonal or a non-orthogonal fiber parallel material frame. This fiber parallel frame is necessary, as rigid body motion predicted by conventional objective rates lead to a mismatch between the corresponding reference frame and fiber orientation for large shear deformation [9,11,21,22]. The applied material frames are based on the work of Hagège [23], Willems [9] and Badel et al. [21] on the application of hypoelastic constitutive laws for large deformation and strong anisotropy. An alternative elastic approach is presented by Peng and Cao [22] using conventional material frames and a suitable transformation of the stiffness tensor. As shown by several authors [10,11,21], however this approach can lead to artificial strains under shear deformation and is therefore not considered.

The fiber parallel frames are adopted and enhanced in this work for modeling viscoelastic bending behavior decoupled from membrane behavior using an orthotropic Voigt-Kelvin and a generalized Maxwell approach. The approaches are consistent with the work of Zienkiewicz et al. [24], Vidal-Sallé [25] and Rösner [26] on mechanical creep analysis. The bending model is implemented for an implicit and an explicit time integration scheme in the commercially available FE solver Abaqus™. The implicit time integration is applied for the parametrization of the model and the explicit time integration for forming simulation, using the iso-thermal forming simulation framework implemented in several user-subroutines as presented by Dörr et al. [27,28].

In the seccond part of this paper, the bending models are parametrized by means of characterization results of a thermoplastic preimpregnated tape (PA6-CF), which are conducted at the ThermoPlastic composites Research Center (TPRC) in Enschede (NL) by the characterization setup presented by Sachs [19].

In the third part, the parameterized bending models are applied to a numerical hemisphere test, to investigate the influence of the presented modeling approaches on the prediction of wrinkling behavior. Finally, the bending model is applied to the forming simulation of a more complex generic geometry and compared to experimental tests, finished at Fraunhofer ICT (Germany).

2. Finite strain viscoelastic bending model

As mentioned above, a basic requirement on constitutive laws describing the intra-ply mechanisms in FE forming simulation is the decoupling of membrane and bending behavior. Therefore, deformation behavior of a single ply is modeled by applying membrane elements overlaid with conventional shell elements, to facilitate the decoupling of membrane and bending behavior. It has to be taken into account, that shell elements consist of a membrane and a plate part, where only the plate part may be considered in the shell elements. Based on the applied shell theory, a shell element may also contain a transversal shear stiffness, which is not considered in the following, as the presented bending model is based solely on the plate part of the shell element. Considering these aspects, a suitable integration scheme and corresponding constitutive equations are presented in the following.

2.1. Integration scheme decoupled bending behavior

Following shell theory, there is a thickness-based relation between membrane forces $\boldsymbol{N}$ and bending moments $\boldsymbol{M}$, resulting from the integration of the Cauchy stress tensor $\boldsymbol{\sigma}(z)$ at the gauss points of the finite element over the initial thickness t_0 of the shell element by [29]

$$\boldsymbol{N} = \int_{t_0} \{\boldsymbol{\sigma}(z)\bar{f}_{33}\}dz, \tag{1}$$

$$\boldsymbol{M} = \int_{t_0} \{\boldsymbol{\sigma}(z)\bar{f}_{33}^2 z\}dz. \tag{2}$$

The deformation gradient in thickness direction $\bar{f}_{33}$ results from the incompressibility assumption imposed based on the in-plane deformation:

$$\bar{f}_{33} = \frac{1}{\bar{f}_{11}\bar{f}_{22} - \bar{f}_{12}\bar{f}_{21}}, \tag{3}$$

where $\bar{f}_{ij}$ $(i,j = 1,2)$ are the in-plane components of the deformation gradient.

For the description of the strain tensor over the thickness of the shell element, a linear approach is sufficient, as the presented approach is applied to describe bending behavior of a single ply with a high slenderness ratio. Hence, no higher order or discontinuous approach is necessary. Therefore, following Koiter-Sanders shell theory [29], the strain tensor is determined by a linear superposition of membrane strain $\bar{\boldsymbol{\varepsilon}}$ and bending strain $\check{\boldsymbol{\varepsilon}}$, where the bending strain is determined by means of the curvature tensor $\boldsymbol{\kappa}$ of the mid-face and the initial distance z^0 to the mid-face, leading to the strain tensor as a linear function of the initial distance to the mid-face:

$$\boldsymbol{\varepsilon}(z^0) = \bar{\boldsymbol{\varepsilon}} + \underbrace{\bar{f}_{33} z^0 \boldsymbol{\kappa}}_{\check{\boldsymbol{\varepsilon}}}. \tag{4}$$

The Cauchy stress tensor $\boldsymbol{\sigma}$ is determined by means of the constitutive equations depending on the distance to the mid-face. For the decoupling of membrane and bending behavior by superimposed membrane and shell elements, only the bending moments according to Eq. (2) are considered in the shell elements. Therefore, bending behavior is implemented in a (V)UGENS-subroutine, which receives membrane strains and curvature tensor as input and delivers membrane forces (Eqn. (1)) and bending moments (Eqn. (2)) back to the solver. Thus, the decoupling of membrane and bending behavior is facilitated by superimposed built-in membrane elements and a shell elements, where only the bending moments are included.

2.2. Conventional material frames and constitutive equations

Another requirement in FE forming simulation is the consideration of geometric non-linearity due to rigid body motion and large deformation, which mainly results from large shear strains. To account for rigid body motion of the material during forming, it has to be ensured that the stress is described within a material fixed frame, the so-called co-rotational frame, which rotates with the material if it undergoes a rigid body motion. Therefore, an objective rate of the stress tensor $\boldsymbol{\sigma}^{\triangledown}$ is introduced, which describes the stress rate of the stress state $\boldsymbol{\sigma}$ within a material fixed frame for an arbitrary rigid body rotation $\mathbf{Q}$ of this frame by

$$\boldsymbol{\sigma}^{\triangledown} = \mathbf{Q} \cdot \left(\frac{\mathrm{d}}{\mathrm{d}t} \left(\mathbf{Q}^{\mathrm{T}} \cdot \boldsymbol{\sigma} \cdot \mathbf{Q} \right) \right) \cdot \mathbf{Q}^{\mathrm{T}}. \tag{5}$$

Denoting the corresponding spin as $\boldsymbol{\Omega} = \dot{\mathbf{Q}} \cdot \mathbf{Q}^{\mathrm{T}}$, the objective stress derivative can be rewritten as [30]

$$\boldsymbol{\sigma}^{\triangledown} = \dot{\boldsymbol{\sigma}} - \boldsymbol{\Omega} \cdot \boldsymbol{\sigma} - \boldsymbol{\sigma} \cdot \boldsymbol{\Omega}^{\mathrm{T}}. \tag{6}$$

A general approach in FE analysises for modeling elastic material behavior and considering geometric non-linearity is based on rate constitutive equations. Therefore, a so-called hypoelastic constitutive equation is given by [30,31]

$$\boldsymbol{\sigma}^{\triangledown}_{\{^t e\}} = \mathbb{C} : \boldsymbol{D}_{\{^t e\}}, \tag{7}$$

where $\mathbb{C}$ is the fourth order elasticity tensor and $\boldsymbol{D}$ the rate of deformation tensor, which represents the strain rate ($\boldsymbol{D} = \dot{\boldsymbol{\varepsilon}}$). The objectivity of the stress rate $\boldsymbol{\sigma}^{\triangledown}$ according to Eq. (5) is guaranteed by expressing the constitutive law within a co-rotational frame $\{^t\boldsymbol{e}\}$ given by

$$^t\boldsymbol{e} = {}^t\mathbf{Q} \cdot {}^0\boldsymbol{e}. \tag{8}$$

For conventional shell elements in Abaqus, Green-Naghdi's objective rate [30] is applied, wherefore the rigid body motion $\mathbf{Q}$ is determined according to the so-called polar decomposition of the deformation gradient $\boldsymbol{F}$, which is given by [30]

$$\boldsymbol{F} = \boldsymbol{R} \cdot \boldsymbol{U} = \boldsymbol{V} \cdot \boldsymbol{R}. \tag{9}$$

This leads to the symmetric right ($\boldsymbol{U}$) or left ($\boldsymbol{V}$) stretch tensor by a rotation of the deformation gradient by the orthogonal rotation tensor. With respect to Eqs. (6) and (8) it follows $\mathbf{Q} = \boldsymbol{R}$ for Green-Naghdi's frame (cf. Fig. 1).

For the application of Green-Naghdi's frame to FE forming simulation, it has to be considered, that rigid body motion predicted by polar decomposition is not unambiguously related to the rotation of the principal material directions of the composite. This issue can be deduced directly from the determination of the fiber orientation $\boldsymbol{a}$ in the deformed configuration on basis of the deformation gradient $\boldsymbol{F}$ and the fiber orientation $\boldsymbol{a}^0$ in the initial configuration by

$$\boldsymbol{a} = \boldsymbol{F} \cdot \boldsymbol{a}^0 = \boldsymbol{V} \cdot \boldsymbol{R} \cdot \boldsymbol{a}^0. \tag{10}$$

Herewith, the initial fiber orientation is rotated to Green-Naghdi's frame by $\boldsymbol{R}$ and subsequently transformed by $\boldsymbol{V}$ within Green-Naghdi's frame. If only normal deformations are present, the fiber orientation vector will only change in length due to the transformation by the left stretch tensor. On the other hand, if also shear deformation is present, the fiber orientation vector will besides a change in length also undergo a rotation within Green-Naghdi's frame.

As shear deformation is the intrinsic deformation mechanism of composites, leading to a misalignment between fiber orientation and the material frame predicted by polar decomposition during forming, a suitable approach has to be found to describe the material behavior within Green-Naghdi's frame, which is necessary to conform to Abaqus conventions. Accordingly, a suitable fiber parallel frame is introduced, which is applied for the elastic and viscoelastic rate constitutive equations presented subsequently.

2.3. Fiber parallel frames

In general, the fiber parallel frame, which is applied for the implementation of the elastic and viscoelastic constitutive equations for large shear deformation presented in the subsequent chapters, is described as a curvilinear frame. This offers the possibility to introduce an either orthogonal or a non-orthogonal material frame. Thus, the approach is applicable to model bending behavior for arbitrary fiber rotations due to shear deformation for a unidirectional or a bidirectional/woven reinforcement, respectively (cf. Fig. 1).

2.3.1. Non-orthogonal frame

For the non-orthogonal approach, the elastic or viscoelastic rate constitutive equations are evaluated within the curvilinear fiber parallel material frame (cf. Fig. 1) with respect to the normalized covariant base vectors $\boldsymbol{g}_{ni}$ and the corresponding dual contravariant base vectors $\boldsymbol{g}^i_n$. As stresses and strains are considered in the user-subroutine within Green-Naghdi's frame, a suitable transformation tensor has to be found, which transforms the base vectors of Green-Naghdi's frame $\{\boldsymbol{e}_i\}$ to the base vectors of the non-orthogonal fiber parallel frame $\{\boldsymbol{g}_{ni}\}$:

$$\{\boldsymbol{g}_{ni}\} = \boldsymbol{U}_n \cdot \{\boldsymbol{e}_i\}, \tag{11}$$

where $\boldsymbol{U}_n$ denotes the normalized right stretch tensor. The normalized right stretch tensor is evaluated on basis of the normalized covariant base within Green-Naghi's frame $\{\boldsymbol{e}_i\}$, which is determined by

$$\boldsymbol{g}_{ni\{\boldsymbol{e}_i\}} = \frac{\boldsymbol{U}_{\{\boldsymbol{e}_i\}} \cdot \boldsymbol{e}_{i\{\boldsymbol{e}_i\}}}{\left\| \boldsymbol{U}_{\{\boldsymbol{e}_i\}} \cdot \boldsymbol{e}_{i\{\boldsymbol{e}_i\}} \right\|}, \tag{12}$$

where $\boldsymbol{U}$ is the in-plane right stretch tensor supplied by the user-subroutine. Herewith, the components of the normalized right stretch tensor are determined by

$$[\boldsymbol{U}_n]_{\{\boldsymbol{e}_i \otimes \boldsymbol{g}_{nj}\}} = \boldsymbol{g}_{nj} \cdot \boldsymbol{e}_i, \tag{13}$$

leading to a transformation between Green-Naghdi's and the fiber parallel frame. Furthermore, the desired correlation of considering arbitrary fiber rotation due to in-plane shear deformation in the

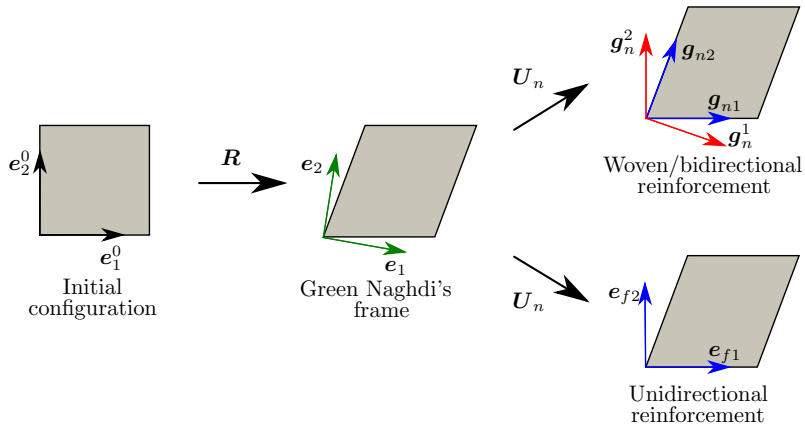

Fig. 1. Schematic illustration of the non-orthogonal/orthogonal fiber parallel material frame and Green-Naghdi's frame due to simple-shear deformation.

bending model is achieved by expressing the constitutive equations in the fiber parallel frame. Fiber rotation due to a torsional deformation of the shell element is not considered, as the influence is expected to be low.

2.3.2. Orthogonal frame

For the orthogonal approach, solely the applied base vectors of the non-orthogonal frame $\{\boldsymbol{g}_{ni}\}$ for the determination of the transformation tensor (Eqn. (13)) have to be replaced by the base vectors of the orthogonal frame $\{\boldsymbol{e}_{fi}\}$, which are determined from:

$$\boldsymbol{e}_{f1} = \boldsymbol{g}_{n1}, \tag{14}$$

$$\boldsymbol{e}_{f2} = \frac{\boldsymbol{g}_{n2} - (\boldsymbol{g}_{n1} \cdot \boldsymbol{g}_{n2})\boldsymbol{g}_{n1}}{\|\boldsymbol{g}_{n2} - (\boldsymbol{g}_{n1} \cdot \boldsymbol{g}_{n2})\boldsymbol{g}_{n1}\|}. \tag{15}$$

2.4. Elastic approach

To model bending behavior in composite forming simulation with an elastic approach, the hypoelastic constitutive law given in Eq. (7) is expressed in the fiber parallel frame:

$$[\boldsymbol{\sigma}^{\nabla}]_{\{\boldsymbol{g}_{ni}\otimes\boldsymbol{g}_{nj}\}} = [\mathbb{C}]_{\{\boldsymbol{g}_{ni}\otimes\boldsymbol{g}_{nj}\otimes\boldsymbol{g}_{nk}\otimes\boldsymbol{g}_{nl}\}} : [\boldsymbol{D}]_{\{\boldsymbol{g}_n^k\otimes\boldsymbol{g}_n^l\}}. \tag{16}$$

For the implementation of this constitutive equation, the generally applied time integration scheme for hypoelastic constitutive laws proposed by Hughes and Winget [31] is adopted, leading to the Cauchy stress in the fiber parallel system given by

$$\left[{}^{t+dt}\boldsymbol{\sigma}\right]_{\{\boldsymbol{g}_{ni}\otimes\boldsymbol{g}_{nj}\}} = \left[{}^{t}\boldsymbol{\sigma}\right]_{\{\boldsymbol{g}_{ni}\otimes\boldsymbol{g}_{nj}\}} + \left[{}^{t+dt}\Delta\boldsymbol{\sigma}\right]_{\{\boldsymbol{g}_{ni}\otimes\boldsymbol{g}_{nj}\}}. \tag{17}$$

The stress increment $\Delta\boldsymbol{\sigma}$ is obtained from the evaluation of the elastic constitutive law on basis of the strain increment $\Delta\boldsymbol{\varepsilon}$ in the fiber parallel system by

$$\left[{}^{t+dt}\Delta\boldsymbol{\sigma}\right]_{\{\boldsymbol{g}_{ni}\otimes\boldsymbol{g}_{nj}\}} = [\mathbb{C}]_{\{\boldsymbol{g}_{ni}\otimes\boldsymbol{g}_{nj}\otimes\boldsymbol{g}_{nk}\otimes\boldsymbol{g}_{nl}\}} : \left[{}^{t+dt}\Delta\boldsymbol{\varepsilon}\right]_{\{\boldsymbol{g}_n^k\otimes\boldsymbol{g}_n^l\}}. \tag{18}$$

The components of the elastic stiffness tensor $\mathbb{C}$ are usually kept constant, but also can be modified to account for non-linear material behavior depending on e.g. curvature.

Based on the normalized right stretch tensor $\boldsymbol{U}_n$, the strain increment within Green-Naghdi's frame can be transformed by

$$\left[{}^{t+dt}\Delta\boldsymbol{\varepsilon}\right]_{\{\boldsymbol{g}_n^i\otimes\boldsymbol{g}_n^j\}} = [\boldsymbol{U}_n]^{T}_{\{\boldsymbol{e}_i\otimes\boldsymbol{g}_{nj}\}} \cdot \left[{}^{t+dt}\Delta\boldsymbol{\varepsilon}\right]_{\{\boldsymbol{e}_i\otimes\boldsymbol{e}_j\}} \cdot [\boldsymbol{U}_n]_{\{\boldsymbol{e}_i\otimes\boldsymbol{g}_{nj}\}}, \tag{19}$$

to the fiber parallel frame. Herewith, the hypoelastic constitutive law is evaluated, leading to the stress increment (Eqn. (18)) and the total stress (Eqn. (17)) in the fiber parallel frame. The total stress with respect to Green-Naghdi's frame is obtained by

$$\left[{}^{t+dt}\boldsymbol{\sigma}\right]_{\{\boldsymbol{e}_i\otimes\boldsymbol{e}_j\}} = [\boldsymbol{U}_n]_{\{\boldsymbol{e}_i\otimes\boldsymbol{g}_{nj}\}} \cdot \left[{}^{t+dt}\boldsymbol{\sigma}\right]_{\{\boldsymbol{g}_{ni}\otimes\boldsymbol{g}_{nj}\}} \cdot [\boldsymbol{U}_n]^{T}_{\{\boldsymbol{e}_i\otimes\boldsymbol{g}_{nj}\}}. \tag{20}$$

The bending moment at the end of the increment within the fiber parallel frame is obtained from the total bending moment at the beginning of the increment and the integration of the stress increment over the thickness of the shell element by:

$${}^{t+dt}\boldsymbol{M}_{\{\boldsymbol{g}_{ni}\otimes\boldsymbol{g}_{nj}\}} = {}^{t}\boldsymbol{M}_{\{\boldsymbol{g}_{ni}\otimes\boldsymbol{g}_{nj}\}} + \int_{t_0}\left({}^{t+dt}\Delta\boldsymbol{\sigma}_{\{\boldsymbol{g}_{ni}\otimes\boldsymbol{g}_{nj}\}}\right)\bar{f}_{33}^2 z\,dz. \tag{21}$$

Therefor a numerical approximation by e.g. Gaussian quadrature can be applied. If there is no dependency between the elastic constants and the stress or strain tensor in form of non-linear material properties, membrane strains can be omitted for the evaluation of the constitutive laws, due to symmetry conditions of the integrand in Eq. (21). Therefore, a closed form solution is obtained for a linear-elastic constitutive law for the incremental bending moment by:

$$\left[{}^{t+dt}\Delta\boldsymbol{M}\right]_{\{\boldsymbol{g}_{ni}\otimes\boldsymbol{g}_{nj}\}} = \left([\mathbb{C}]_{\{\boldsymbol{g}_{ni}\otimes\boldsymbol{g}_{nj}\otimes\boldsymbol{g}_{nk}\otimes\boldsymbol{g}_{nl}\}} : \left[{}^{t+dt}\Delta\boldsymbol{\kappa}\right]_{\{\boldsymbol{g}_n^k\otimes\boldsymbol{g}_n^l\}}\right)\frac{t_0^3\bar{f}_{33}^2}{12}, \tag{22}$$

based on the increment of the curvature tensor $\Delta\boldsymbol{\kappa}$ in the fiber parallel frame. The total bending moment at the end of the increment within Green Naghdi's frame, which has to be passed back to the solver, is obtained in analogy to Eq. (20).

2.5. Viscoelastic approaches

The viscoelastic bending model is implemented using a generalized Maxwell and a Voigt-Kelvin approach, where the constitutive equations are implemented within the fiber parallel frames, in analogy to the elastic approach introduced above.

2.5.1. Generalized Maxwell approach

A so-called generalized Maxwell model has proven to be useful to describe rate- and time-dependent material characteristics. With regard to a symbolic illustration, a generalized Maxwell model is composed of a spring arranged in parallel with an arbitrary number of spring-dashpot elements (cf. Fig. 2(a)). The relations for the stresses and strains are given by

$$\boldsymbol{\sigma} = \boldsymbol{\sigma}_0 + \sum_{i=1}^{N}\{\boldsymbol{\sigma}_i\}, \tag{23}$$

$$\boldsymbol{\varepsilon} = \boldsymbol{\varepsilon}_i = \boldsymbol{\varepsilon}_i^e + \boldsymbol{\varepsilon}_i^v, \tag{24}$$

where the stress tensor $\boldsymbol{\sigma}$ is additively composed from the purely elastic stress $\boldsymbol{\sigma}_0$ and the internal viscoelastic stress variables $\boldsymbol{\sigma}_i$. On the contrary, the total strain is equal for each spring- and spring-dashpot-element. Within a spring-dashpot-element, the total strain is sumperimposed from an elastic $\boldsymbol{\varepsilon}_i^e$ and a viscous part $\boldsymbol{\varepsilon}_i^v$.

For the spring-element, the hypoelastic approach presented in the previous chapter is applied. The constitutive law for the spring-dashpot-elements within a material fixed frame $\{\boldsymbol{e}_i\}$ is given by

$$\dot{\boldsymbol{\varepsilon}}_i = \mathbb{S}_i : \boldsymbol{\sigma}_i^{\nabla} + \mathbb{V}_i^{-1} : \boldsymbol{\sigma}_i, \tag{25}$$

where $\dot{\boldsymbol{\varepsilon}}_i$ is the strain rate, $\mathbb{S}_i$ the fourth order compliance tensor, $\boldsymbol{\sigma}_i^{\nabla}$ the stress rate, $\mathbb{V}_i^{-1}$ the fourth order viscosity tensor and $\boldsymbol{\sigma}_i$ the internal stress tensor of a spring-dashpot-element. The usually applied separation of volumetric and distortional strains has not to be taken into account, as material behavior is modeled incompressible by adjusting the thickness of the shell element according to the in-plane deformation (Eqn. (3)).

For the implementation, a central-differential-operator is applied to discretize the differential equation of the constitutive law in time. This leads to the incremental stress tensor, which is evaluated within the fiber parallel frame $\{\boldsymbol{g}_{ni}\}$:

$${}^{t+dt}\Delta\boldsymbol{\sigma}_i = \left(\mathbb{S}_i + \mathbb{V}_i^{-1}\frac{\Delta t}{2}\right)^{-1} : \left({}^{t+dt}\Delta\boldsymbol{\varepsilon} - \mathbb{V}_i^{-1} : {}^{t}\boldsymbol{\sigma}_i\Delta t\right), \tag{26}$$

where Δt is the time increment and $\Delta\boldsymbol{\varepsilon}$ the strain increment. Based on the incremental stress tensor $\Delta\boldsymbol{\sigma}_l$ for each spring-dashpot

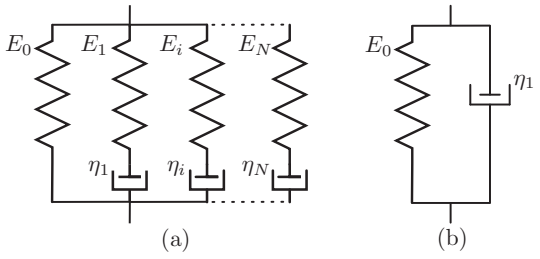

Fig. 2. Symbolic illustration of a generalized Maxwell (a) and a Voigt-Kelvin model (b).

element, the total bending moment in the fiber parallel frame at the end of the increment is obtained by

$$ {}^{t+dt}[\boldsymbol{M}]_{\{\boldsymbol{g}_{ni}\otimes\boldsymbol{g}_{nj}\}} = {}^{t}[\boldsymbol{M}]_{\{\boldsymbol{g}_{ni}\otimes\boldsymbol{g}_{nj}\}} + \sum_{l=0}^{N}\left\{\int_{t_0}\left({}^{t+dt}[\Delta\boldsymbol{\sigma}]_{l\{\boldsymbol{g}_{ni}\otimes\boldsymbol{g}_{nj}\}}\right)\bar{f}_{33}^{2}z\mathrm{d}z\right\}, \tag{27} $$

which is transformed to Green-Naghdi's frame in analogy to the elastic approach.

2.5.2. Voigt-Kelvin-approach

A Voigt-Kelvin-approach, consisting of a spring-element in parallel connected with a single dashpot-element (cf. Fig. 2(b)), is directly obtained from reducing the integration scheme of a spring-dashpot-element by the elastic stiffness (Eq. 26), leading to the incremental viscous stress, evaluated in the fiber parallel frame $\{\boldsymbol{g}_{ni}\}$:

$$ {}^{t+dt}\Delta\boldsymbol{\sigma}^{V} = \left(\frac{2}{\Delta t}\right)\mathbb{V} : \left({}^{t+dt}\Delta\boldsymbol{\varepsilon} - \mathbb{V}^{-1} : {}^{t}\boldsymbol{\sigma}\Delta t\right) \tag{28} $$

In analogy to the generalized Maxwell approach, the total bending moment is determined within the fiber parallel frame (Eqn. (27)), which is subsequently transformed to Green Naghdi's frame.

3. Parametrization of the bending model for thermoplastic UD-Tapes

3.1. Material characterization

The bending characterization is conducted at TPRC in the Netherlands, wherefore the rheometer bending setup presented by Sachs [19] (cf. Fig. 3) is applied for the characterization of bending properties of a single ply of unidirectional reinforced (UD) PA6-CF tape. The custom fixture, which is mounted on a standard rheometer within a thermal chamber, facilitates the characterization of the rate-dependent bending behavior by prescribing a controlled rotation speed for the rotating upper shaft of the rheometer. The specimen is oriented such that the specimen is deflected along fiber direction. For the iso-thermal investigation of the bending properties, the characterization is conducted at 260 °C, which is a characteristic forming temperature for a PA6-CF tape and which is well above the melting temperature of the thermoplastic.

Fig. 4 depicts the characterization results for three rotation speeds, where the rotating shaft is deflected up to an angle of 1.2 rad. The progression of the curves for the different speeds reveals the distinct rate-dependent bending behavior. The initial overshot of the bending moments for the high rotation speed is referable to inertia effects. At higher deflection angles, irregularities of the measured bending moments are observed, which are attributable to sticking and frictional effects within the fixture.

3.2. Parameter identification

3.2.1. Simulation of the rheometer bending test

For the determination of the parameters for the bending model according to the characterization results, the rheometer bending test is modeled using an implicit dynamic finite element analysis based on Newton's method. This procedure is applied to guarantee numerical efficiency, compared to an explicit analysis, as the characterization test for the low rotation speed lasts up to 50 s.

The bending models presented in the previous chapter are implemented in a UGENS-subroutine for modeling the bending behavior of the specimen, based on the built-in finite strain shell elements (S4R). It should be noted, that these element type includes a transversal shear stiffness, which is not modifiable by UGENS-subroutine. Hence, the Abaqus built-in approach for modeling transversal shear stiffness has to be applied. It turns out, that transversal shear stiffness has no distinct influence on bending behavior, if the assigned value is chosen small enough. Thus, a small isotropic transversal shear stiffness is assigned and the bending characteristic is modeled solely via the plate part of the shell element according to the approaches presented in Section 2.

Furthermore, it should be noted that with the characterization method only bending behavior along fiber direction is characterized. As no coupling terms are included in the stress-strain-relation, the stress state reduces to an uniaxial stress state. For the modeling of the characterization set-up, therefore the material properties in transverse direction have no influence on the obtained bending moments.

3.2.2. Parameter optimization algorithm and error measure

The optimization algortihm presented by Nelder and Mead [32] is adopted for material parameter extraction and implemented based on the Abaqus-Python-interface. As error measure for the optimization procedure, the normalized summed squared error given by

$$ RSSN = \frac{1}{n}\sum_{i=1}^{n}\left(\frac{\left(\widehat{M}_{b,i} - M_{b,i}\right)^{2}}{M_{b,i}^{2}}\right), \tag{29} $$

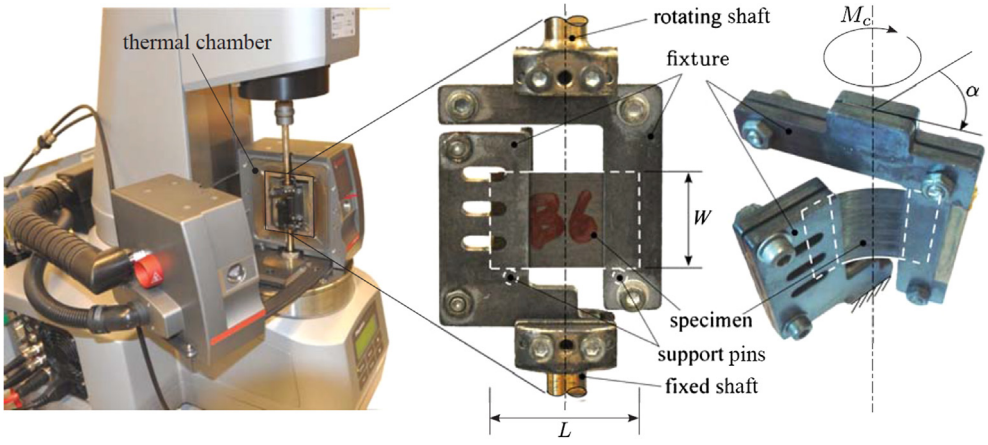

Fig. 3. Experimental set-up for the characterization of bending properties for thermoplastic UD-Tapes, mounted in an Anton Paar MCR501 rheometer and a CTD 450 thermal chamber [19].

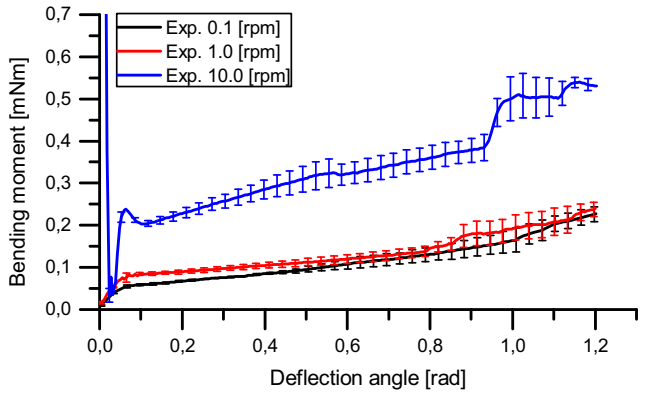

Fig. 4. Experimental bending results for a single ply PA6-CF UD-Tape for different rotation speeds at 260 °C.

is applied, where $\widehat{M}_{b,i}$ and $M_{b,i}$ are the bending moment values determined in the FEA and in the characterization test, respectively. The parameters manipulated by the optimization tool-box are the elastic and viscous properties of the approaches presented above, whereas transversal shear stiffness is kept at a constant small value.

In the following, only the deflections lower than 0.5 rad are considered, as only in this range no irregularities due to slipping and sliding are observed and the standard deviations of the two lower angular velocities do not cross each other. Furthermore, the overshot at the beginning for the high rotation speed is neglected for the parameter identification.

3.2.3. Results of the elastic approach

Fig. 5(a) and (b) reveal that the bending characteristic of the thermoplastic UD-Tapes at process conditions is not describable with a purely elastic approach. Fig. 5(a) depicts the obtained result by application of the fitting procedure described above, whereas 5 (b) depicts the results based on a parameter set, which is determined by fitting the parameters to the "initial stiffness" of the bending characterization. Both of these material parameter sets are applied to a numerical study of a hemisphere test, presented in the next chapter.

3.2.4. Results of the Voigt-Kelvin approach

For the Voigt-Kelvin approach, a constant parameter for the spring element and rate-dependent parameters for the dashpot-element are determined for each curve (cf. Table 1), leading to a good agreement between characterization and simulation results for the two lower rotations speeds and a mismatch for the high rotation speed (cf. Fig. 5(c)). Hence, at least the parameter for viscosity has to vary with the rotation speed to obtain an approximate agreement with the Voigt-Kelvin approach. Since it can be shown that the deformation rate is approximately constant during the bending testby an FE analysis, a so-called cross-viscosity fluid is suitable to describe viscosity parameters for the bending behavior depending on the deformation rate $\dot{\gamma}$ according to [33]

$$\eta(\dot{\gamma}) = \frac{\eta_0 - \eta_\infty}{1 + m\dot{\gamma}^{(1-n)}} + \eta_\infty. \tag{30}$$

3.2.5. Results of the generalized Maxwell approach

For the application of the generalized Maxwell model, a single spring-element in parallel with two Maxwell elements is applied to guarantee numerical efficiency, as the application of more than two Maxwell elements show only a marginal improvement of the simulation results. In analogy to the Voigt-Kelvin approach, it is observed that bending behavior is not predictable with a linear generalized Maxwell model with constant parameters, as for a linear generalized Maxwell model the obtained bending moments scale proportionally with the deformation rate. Therefore, a nonlinear viscosity according to a hyperbolic sine law is introduced for the dashpot elements:

$$\eta_i = A_i \cdot \sinh\left(m_i \cdot \bar{\sigma}_i\right)^{n_i}, \tag{31}$$

where A_i, m_i and n_i are the material properties in each Maxwell element. The internal stress invariant $\bar{\sigma}_i$ within each Maxwell element is evaluated in the fiber parallel frame according to

$$\bar{\sigma}_i = \sqrt{\boldsymbol{\sigma}_{i\{\boldsymbol{g}_{n\circ}\}} : \boldsymbol{\sigma}_{i\{\boldsymbol{g}_{n\circ}\}}}. \tag{32}$$

Fig. 5(d) reveals, that a good agreement between simulation and characterization tests is achieved for the generalized Maxwell approach with a non-linear viscous behavior. This is obvious, as the varying slope of the curves is modeled well for each deformation rate. Also the progression of the curves at the beginning of the test is better represented than by the Voigt-Kelvin approach.

4. Application and evaluation of the bending model in FE forming simulation

For the forming simulation using the commercially available FE solver Abaqus, an explicit time integration scheme is applied, due to the large contact areas. Bending behavior is modeled using the approaches presented in Section 2 and parametrizations presented in Section 3. As only bending behavior in fiber direction is parametrized, the material properties in transverse direction are approximated by a knock-down factor, leading to a bending stiffness 100-times lower compared to bending stiffness in fiber direction.

4.1. Models for membrane and interface behavior

For the modeling of interface and membrane behavior, suitable constitutive equations are implemented using the so-called VUINTERACTION and VUMAT subroutine, respectively. These approaches and parametrizations are describe in detail by Dörr et al. [27,28] and are outlined only shortly in the following.

4.1.1. Interface behavior

The interface mechanisms at the interfaces between the tool and the laminate, as well as between the single plies of the stacked laminate are regularized using the Penalty method [34]. Beyond that, Penalty stiffness is enhanced to account for adhesion between the adjacent plies of the stacked laminate if a user-defined distance between the surfaces is not exceeded and if the interacting surfaces tend to open.

In tangential direction, frictional behavior is modeled not only in relation to the normal pressure p, but also dependent on the slip-rate v and adhesion τ_0 between the interacting surfaces. Therefore, the critical stress of a conventional Coulomb frictional law $\mu \cdot p$ is enhanced by a slip-rate dependent term $\eta \cdot v$ and by a constant offset term τ_0, leading to the linear constitutive law given by

$$\tau_{crit} = \mu \cdot p + \eta \cdot v + \tau_0. \tag{33}$$

4.1.2. Membrane behavior

To model membrane behavior, the "Ideal Fiber Reinforced Model" (IFRM), presented by Spencer [35,36] and applied to viscous media [37–39] and to FE forming simulation in the Aniform code™ [13], is applied. Following the IFRM, the Cauchy stress tensor for a unidirectional reinforcement is given by

$$\boldsymbol{\sigma} = -p\boldsymbol{I} + T_a \boldsymbol{a} \otimes \boldsymbol{a} + \boldsymbol{\tau}, \tag{34}$$

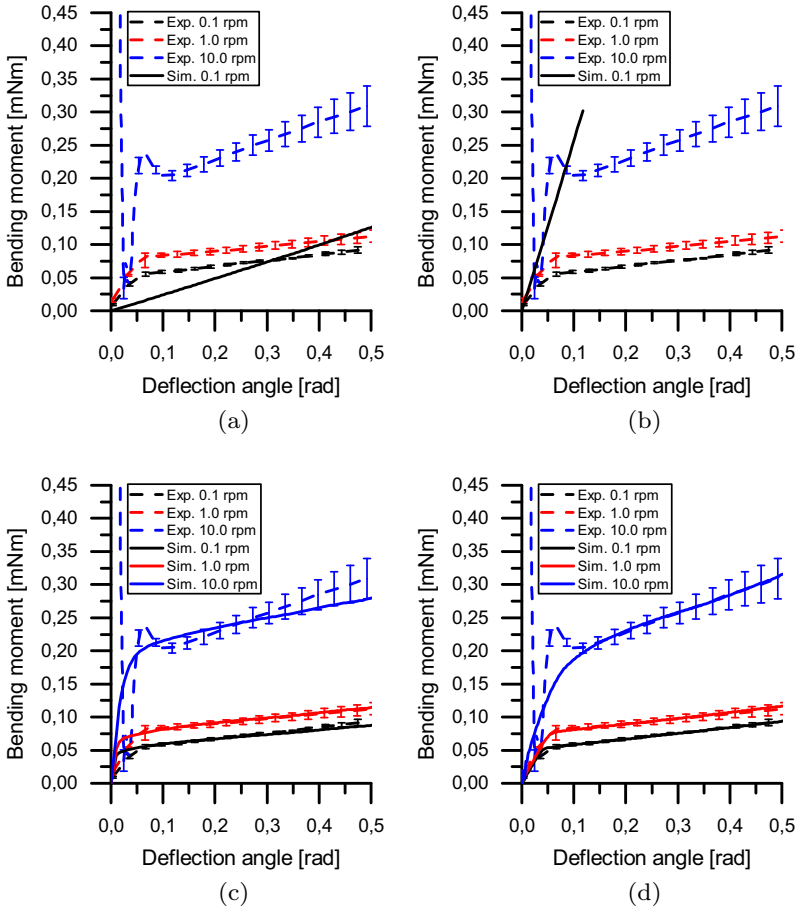

Fig. 5. Comparison of the prediction of the bending models to characterization results for different rotation speeds at 260 °C; (a) Elastic "best-fit", (b) Elastic fitting "initial stiffness", (c) Voigt-Kelvin approach and (d) generalized Maxwell approach.

Table 1
Material parameters for the bending model according to the Voigt-Kelvin-approach fitted to each curve of the bending characterization.

Angular velocity [rpm]	Elastic modulus [MPa]	Viscosity [MPa·s]
0.1	125.0	5550.0
1.0	125.0	775.0
10.0	125.0	250.0

with p as an arbitrary hydrostatic pressure inducing material incompressibility, $\boldsymbol{I}$ the second order identity tensor and T_a as sufficiently high unidirectional stress term, inducing the inextensibility condition in direction of the fibers $\boldsymbol{a}$. $\boldsymbol{\tau}$ is the matrix-related extra stress term, which is adopted for the modeling of an isotropic Voigt-Kelvin approach using a linear elastic spring element and a cross viscosity fluid for the dashpot element.

4.2. Numerical study: hemisphere test

The influence of the different bending models in conjunction with the material parameter sets determined in Section 3 is investigated in a numerical study of a hemisphere test. Forming velocities in a usual range, as well as two different layups are considered. The considered layups namely are a biaxial $[0;90]_s$ layup, leading to a wrinkle-free forming and a triaxial $[45;0;-45]$ layup, leading to severe wrinkling during forming (cf. Fig. 6(b) and (c)).

Considering the forming behavior for the two different layups and an intermediate forming velocity at 50 mm/s (cf. Fig. 6(a)), it turns out that the evolution of curvature rate and curvature evolves very similar for the two considered layups until a tool stroke of approximately 10 mm, which is the forming stage of wrinkling initiation for the triaxial layup. To investigate the influence of the bending models on the wrinkling behavior, the surface curvature is determined for a forming stage where the wrinkles are well developed, which is the case for a remaining tool stroke of 9.5 mm (cf. Fig. 7). It turns out, that the generalized Maxwell approach, the Voigt-Kelvin approach and the elastic approach fitted to the "initial stiffness" lead to similar results. The generalized Maxwell approach leads to the smallest wrinkles, but the position of the wrinkles is the same for the different approaches. On the other hand, the elastic approach according to the "best-fit" leads to differing wrinkling behavior for which the main wrinkles are located at different positions compared to the other approaches. The same behavior is observed in the evolution of the mean surface curvature determined for several forming stages and the different bending modeling approaches (cf. Fig. 8(a)), where especially the generalized Maxwell approach and the Voigt-Kelvin approach lead to very similar results.

In comparison between curvature rates observed in the forming simulation of the hemisphere for a forming velocity of 50 mm/s and the curvature rates observed in the characterization, it turns out that for the biaxial layup mean curvature rate observed in simulation is mostly within the characterized range. The characterized curvature rates range from approximately 0.0005 to 0.05 rad/mm.s and are highlighted in gray (cf. Fig. 6(a)). On the other hand, curvature rates far outside the characterized range are observed after wrinkling initiation and during wrinkling evolution for the triaxial layup. This correlation is only valid for a forming velocity up to

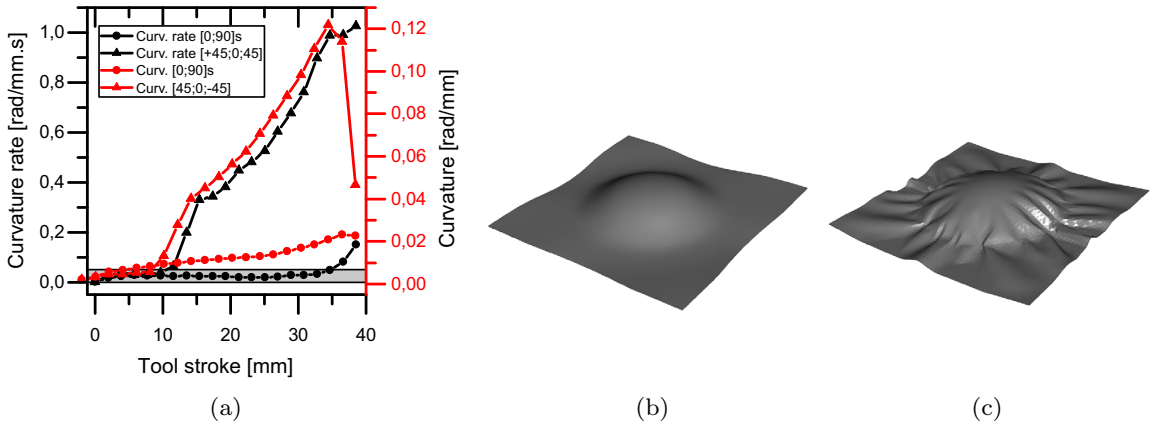

Fig. 6. Mean curvature rate and curvature over the tool stroke for the forming simulations of a hemisphere with a $[0;90]_s$ and a $[45;0;-45]$ layup for the generalized Maxwell approach (a) and the according forming simulation results for a remaining tool stroke of 9.5 mm in (b) and (c), respectively.

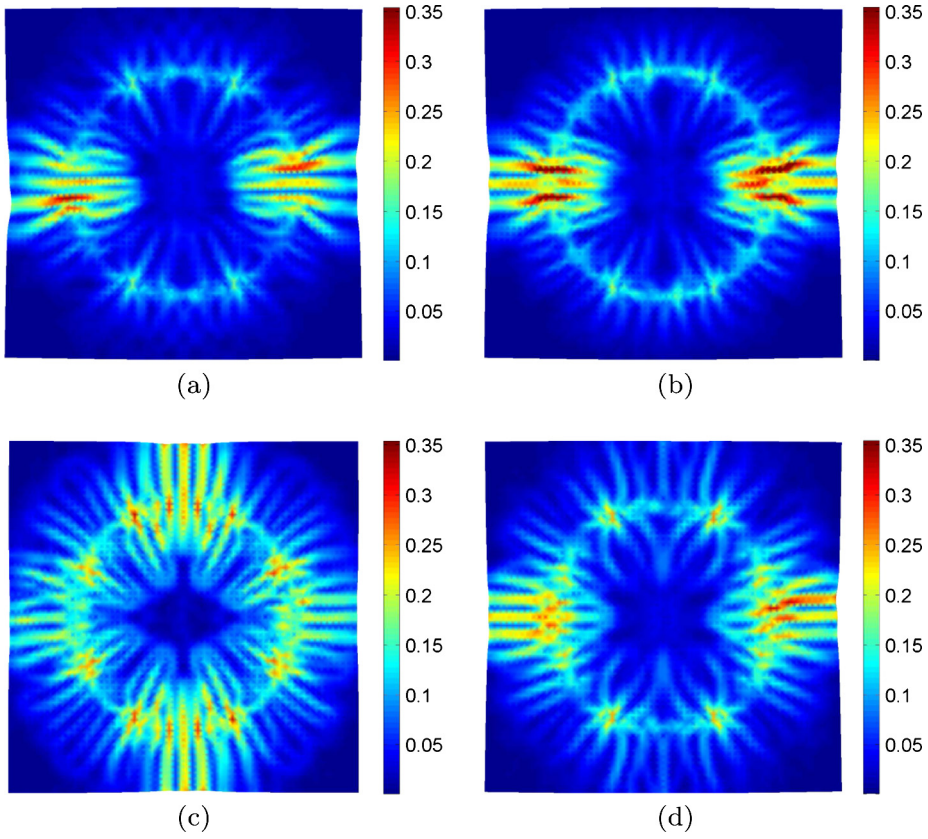

Fig. 7. Surface curvature of a $[45;0;-45]$ layup for a remaining tool stroke of 9.5 mm for the generalized Maxwell approach (a), the Voigt-Kelvin approach (b), the elastic "best-fit" approach (c) and the elastic approach fitted to the "initial bending stiffness" (d).

100 mm/s, which is apparent from the comparison of mean curvature rate before and after wrinkling initiation for a remaining tool stroke of 31 mm and 9.5 mm, respectively (cf. Fig. 8(b)). As the position of the wrinkles is determined by the "initial stiffness", as shown by the two different fitting alternatives for the elastic approach, the characterization range may be sufficient for the prediction of wrinkling locations, in case of the considered hemisphere and for intermediate forming velocities.

4.3. Application test: generic geometry

As an application test, the above presented model for FE forming simulation is applied to a generic and more complex geometry with a $[0;45;-45;90]_s$ layup. The blank is formed without inducing membrane forces by grippers, where the blank is dropped on the lower female tool and the male tool is conducting the tool stroke. Forming simulation is conducted modeling each of the eight single plies, where for the bending behavior the different bending models and the according parameter sets determined in Section 3 are applied in analogy to the numerical hemisphere test. The forming simulation result of the generalized Maxwell approach is compared to the experimental result for a remaining tool stroke of 5 mm, where wrinkles are well developed. A good agreement of position and direction of the wrinkles is observed (cf. Fig. 9(a) and (b)). In comparison between the bending modeling approaches for the same forming state, a similar correlation as for the

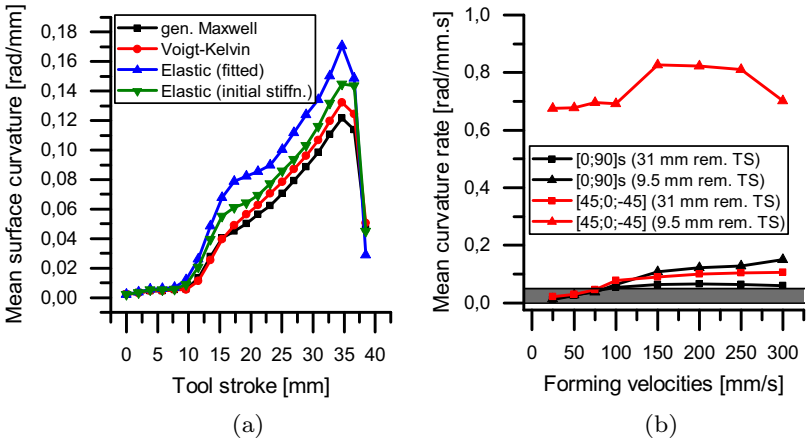

Fig. 8. Mean surface curvature of a $[45; 0; -45]$ layup vs. tool stroke for a forming velocity of 50 mm/s (a) and mean curvature rate for a remaining tool stroke of 9.5 mm and 31 mm for several forming velocities (b).

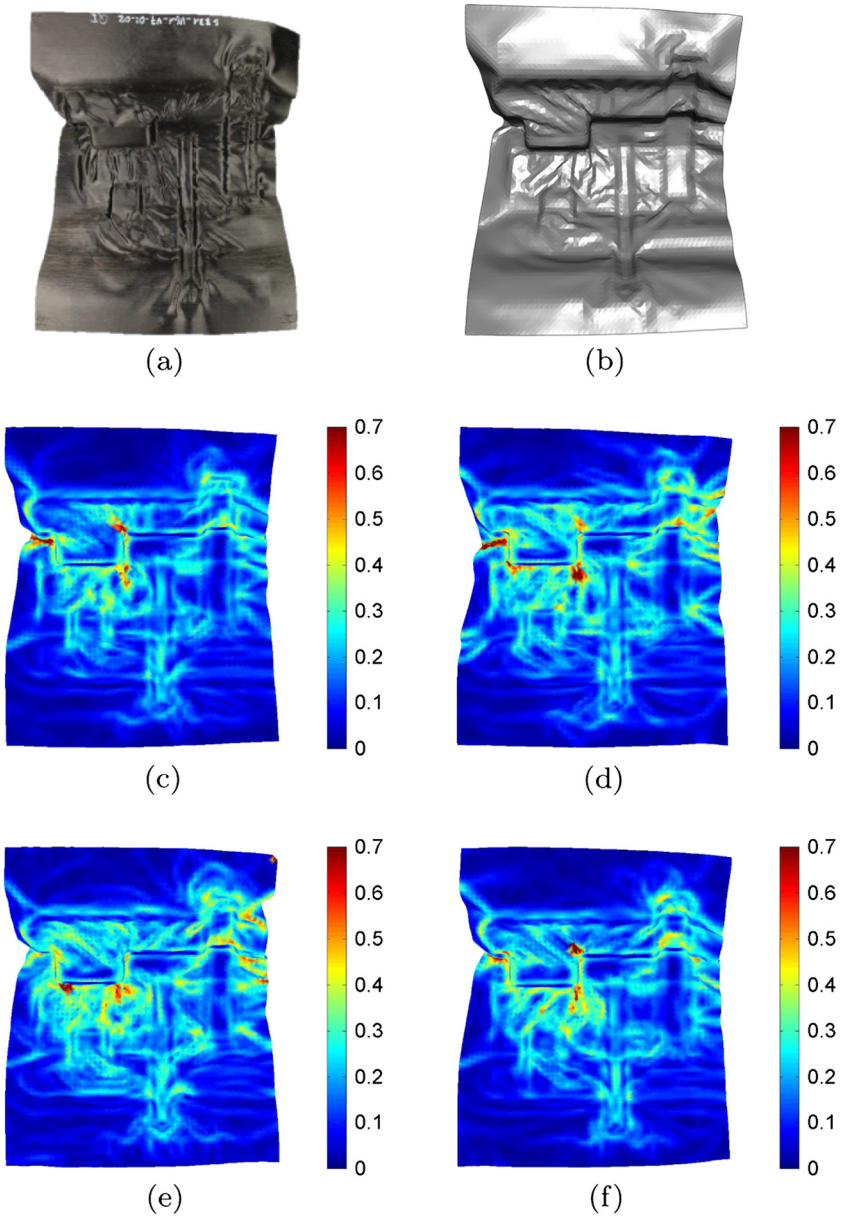

Fig. 9. Comparison of the experimental test (a) to the forming simulation result (b) for a $[0; 45; 90; -45]_s$ layup and a remaining tool stroke of 5 mm and comparison of the according surface curvature for the generalized Maxwell approach (c), the Voigt-Kelvin approach (d), the elastic "best-fit" approach (e) and the elastic approach fitted to the "initial stiffness" (f).

numerical study is observed. Accordingly, the generalized Maxwell, the Voigt-Kelvin and the elastic approach fitted to the "initial stiffness" predict a comparable wrinkling behavior, whereas sharper and more wrinkles are predicted by the elastic "best-fit" (cf. Fig. 9(c)–(f)).

5. Conclusion

Finite strain approaches for modeling viscoelastic bending behavior in FE composite forming simulation are presented, following a purely elastic, a Voigt-Kelvin and a generalized Maxwell approach. The approaches are implemented within the commercially available FE solver Abaqus™ and account for fiber reorientation during forming due to in-plane shear deformation. By introduction of an either orthogonal or non-orthogonal fiber parallel material frame for the evaluation of the constitutive law, it is feasible to model bending behavior for a unidirectional or a bidirectional/woven fiber architecture.

The presented viscoelastic approaches are successfully parameterized according to iso-thermal characterization results of a thermoplastic UD-Tape at process conditions, for which a distinct rate-dependent deformation behavior is observed. It turns out, that only the generalized Maxwell approach in conjunction with non-linear viscous behavior is suitable to predict the bending characteristic completely (Fig. 5(d)). The Voigt-Kelvin approach with non-linear viscous behavior gives only approximate results (Fig. 5(c)). On the contrary, the elastic approach is not suitable to describe the complete characteristic of the dynamic rheometer test. The elastic approach may either describe the "initial stiffness" of the rheometer test (Fig. 5(b)), which is caused by the rate-dependent material behavior, or describe the array of experimental curves via an averaged straight line (Fig. 5(a)).

Finally, the presented bending modeling approaches are applied to forming simulation of a hemisphere and a generic geometry, investigating their capability of predicting wrinkling behavior. Wrinkling in composite forming is an instability issue, determined by the balance between effective shear and effective bending stiffness of the laminate. The onset of wrinkling usually occurs in areas with no or moderate curvatures and curvature rates of the partially formed laminate (Fig. 7). High curvatures and curvature rates are only observed in forming stages where the size of wrinkles have already developed and increased due to closing the mold successively (Figs. 6(a) and 8(a)). The viscoelastic approaches and the elastic approach fitted to the "initial stiffness" of the rheometer test lead to similar locations of wrinkles in forming simulation (Figs. 7 and 9). Hence, the onset of wrinkling is controlled by the "initial bending stiffness" at low curvatures, caused by the rate-dependent material behavior. In comparison, evolution of wrinkling is controlled by the bending stiffness at higher curvatures and higher curvature rates. Therefore, the maximum size of wrinkles in forming simulation varies depending on the applied modeling approach (Fig. 8(a)). Furthermore, the forming simulation result for the generic geometry, obtained with the generalized Maxwell approach, show a good agreement with the presented experimental tests (Fig. 9(a) and (b)).

In summary, modeling viscoelastic bending behavior is crucial to predict wrinkling in FE forming simulation of thermoplastic pre-impregnated tapes. In this context the generalized Maxwell approach in conjunction with non-linear viscous behavior is most suitable to predict the onset of wrinkling as well as wrinkling evolution. However, the presented investigations reveal that a purely elastic approach is capable to predict the onset of wrinkles, if the bending stiffness is fitted to the "initial stiffness" observed in the dynamic rheometer test. Since the rate-dependent material behavior obviously determines the onset of wrinkling, the dynamic bending characterization is crucial for parametrization and modeling of wrinkling behavior. Consequently, it is questionable if the often applied static cantilever test is suitable to characterize the bending behavior of thermoplastic pre-impregnated tapes. However, the above described insights are primarily valid for the iso-thermal investigations and may change if non-isothermal effects are included. This will be a scope of future investigations. Beyond that, modeling of membrane behavior will be considered more precisely in the same context.

Acknowledgment

The authors would like to thank the German Federal Ministry of Education and Research for the funding of the project SMiLE (03X3041P), for which the presented work is carried out. Furthermore, the authors are grateful for the commission and supply of the characterization results by Steffen Ropers (VW AG). As well the authors greatful appreciate the support of Fraunhofer ICT by supplying the experimental forming results of the generic geometry, which were finished under the project leadership of Tobias Joppich.

References

[1] Fuchs E, Field F, Roth R, Kirchain R. Strategic materials selection in the automobile body: economic opportunities for polymer composite design. Compos Sci Technol 2008;68(9):1989–2002. doi: http://dx.doi.org/10.1016/j.compscitech.2008.01.015.

[2] Verrey J, Wakeman MD, Michaud V, Månson J-A. Manufacturing cost comparison of thermoplastic and thermoset rtm for an automotive floor pan. Compos Part A: Appl Sci Manuf 2006;37(1):9–22. doi: http://dx.doi.org/10.1016/j.compositesa.2005.05.048.

[3] Joppich T, Dörr D, Meulen Lvd, Link T, Hangs B, Henning F. Layup and process dependent behavior of pps/cf ud tape-laminates during non-isothermal press forming into a complex component. In: Proceedings ESAFORM 16, Nantes, France.

[4] Kärger L, Bernath A, Fritz F, Galkin S, Magagnato D, Oeckerath A, Schön A, Henning F. Development and validation of a cae chain for unidirectional fibre reinforced composite components. Compos Struct 2015;132:350–8. doi: http://dx.doi.org/10.1016/j.compstruct.2015.05.047.

[5] Lessard H, Lebrun G, Benkaddour A, Pham X-T. Influence of process parameters on the thermostamping of a [0/90]12 carbon/polyether ether ketone laminate. Compos Part A: Appl Sci Manuf 2015;70:59–68. doi: http://dx.doi.org/10.1016/j.compositesa.2014.12.009.

[6] Harrison P, Gomes R, Curado-Correia N. Press forming a 0/90 cross-ply advanced thermoplastic composite using the double-dome benchmark geometry. Compos Part A: Appl Sci Manuf 2013;54:56–69. doi: http://dx.doi.org/10.1016/j.compositesa.2013.06.014.

[7] de Luca P, Lefébure P, Pickett AK. Numerical and experimental investigation of some press forming parameters of two fibre reinforced thermoplastics: apc2-as4 and pei-cetex. Compos Part A: Appl Sci Manuf 1998;29(1–2):101–10. doi: http://dx.doi.org/10.1016/S1359-835X(97)00060-2.

[8] Haanappel SP, ten Thije R, Sachs U, Rietman B, Akkerman R. Formability analyses of uni-directional and textile reinforced thermoplastics. Compos Part A: Appl Sci Manuf 2014;56:80–92. doi: http://dx.doi.org/10.1016/j.compositesa.2013.09.009.

[9] Willems A. Forming simulations of textile reinforced composite shell structures. Phd thesis, KU Leuven, Heverlee (Belgium); 2008.

[10] Badel P, Gauthier S, Vidal-Sallé E, Boisse P. Rate constitutive equations for computational analyses of textile composite reinforcement mechanical behaviour during forming. Compos Part A: Appl Sci Manuf 2009;40(8):997–1007. doi: http://dx.doi.org/10.1016/j.compositesa.2008.04.015.

[11] Khan MA, Mabrouki T, Vidal-Sallé E, Boisse P. Numerical and experimental analyses of woven composite reinforcement forming using a hypoelastic behaviour: application to the double dome benchmark. J Mater Process Technol 2010;210(2):378–88. doi: http://dx.doi.org/10.1016/j.jmatprotec.2009.09.027.

[12] ten Thije R, Akkerman R. A multi-layer triangular membrane finite element for the forming simulation of laminated composites. Compos Part A: Appl Sci Manuf 2009;40(6–7):739–53. doi: http://dx.doi.org/10.1016/j.compositesa.2009.03.004.

[13] Haanappel S. Forming of ud fibre reinforced thermoplastics: a critical evaluation of intra-ply shear Phd thesis. Twente, Enschede, Netherlands: University of Twente; 2013.

[14] Boisse P, Hamila N, Vidal-Sallé E, Dumont F. Simulation of wrinkling during textile composite reinforcement forming: influence of tensile, in-plane shear and bending stiffnesses. Compos Sci Technol 2011;71(5):683–92. doi: http://dx.doi.org/10.1016/j.compscitech.2011.01.011.

[15] Allaoui S, Boisse P, Chatel S, Hamila N, Hivet G, Soulat D, et al. Experimental and numerical analyses of textile reinforcement forming of a tetrahedral shape. Compos Part A: Appl Sci Manuf 2011;42(6):612–22. doi: http://dx.doi.org/10.1016/j.compositesa.2011.02.001.
[16] Guzman-Maldonado E, Hamila N, Boisse P, Bikard J. Thermomechanical analysis, modelling and simulation of the forming of pre-impregnated thermoplastics composites. Compos Part A: Appl Sci Manuf 2015;78:211–22. doi: http://dx.doi.org/10.1016/j.compositesa.2015.08.017.
[17] Soulat D, Cheruet A, Boisse P. Simulation of continuous fibre reinforced thermoplastic forming using a shell finite element with transverse stress. Comput Struct 2006;84(13–14):888–903. doi: http://dx.doi.org/10.1016/j.compstruc.2006.02.011.
[18] Guzman-Maldonado E, Hamila N, Naouar N, Moulin G, Boisse P. Simulation of thermoplastic prepreg thermoforming based on a visco-hyperelastic model and a thermal homogenization. Mater Des 2016;93:431–42. doi: http://dx.doi.org/10.1016/j.matdes.2015.12.166.
[19] Sachs U. Friction and bending in thermoplastic composites forming processes Phd thesis. Twente, Enschede, Netherlands: University of Twente; 2014.
[20] Ropers S, Kardos M, Osswald TA. A thermo-viscoelastic approach for the characterization and modeling of the bending behavior of thermoplastic composites. Compos Part A: Appl Sci Manuf 2016;90:22–32. doi: http://dx.doi.org/10.1016/j.compositesa.2016.06.016.
[21] Badel P, Vidal-Sallé E, Boisse P. Large deformation analysis of fibrous materials using rate constitutive equations. Comput Struct 2008;86(11–12):1164–75. doi: http://dx.doi.org/10.1016/j.compstruc.2008.01.009.
[22] Peng XQ, Cao J. A continuum mechanics-based non-orthogonal constitutive model for woven composite fabrics. Compos Part A: Appl Sci Manuf 2005;36(6):859–74. doi: http://dx.doi.org/10.1016/j.compositesa.2004.08.008.
[23] Hagège B. Simulation du comportement mecanique des milieux fibreux en grandes transformations: application aux renforts tricotes Phd thesis (French). Paris, France: Ecole Nationale Superieure d Arts et Metiers; 2004.
[24] Zienkiewicz OC, Watson M, King IP. A numerical method of visco-elastic stress analysis. Int J Mech Sci 1968;10(10):807–27. doi: http://dx.doi.org/10.1016/0020-7403(68)90022-2.
[25] Vidal-Sallé E, Chassagne P. Constitutive equations for orthotropic nonlinear viscoelastic behaviour using a generalized maxwell model application to wood material. Mech Time-Depend Mater 2007;11(2):127–42. doi: http://dx.doi.org/10.1007/s11043-007-9037-2.
[26] Roesner A. Beschreibung des viskoelastischen und viskoplastischen deformationsverhaltens von kontinuierlich faserverstärktem polyamid-6 Phd thesis (German). Karlsruhe, Germany: KIT; 2015.
[27] Dörr D, Joppich T, Schirmaier F, Mosthaf T, Kärger L, Henning F. A method for validation of finite element forming simulation on basis of a pointwise comparison of distance and curvature. In: Proceedings ESAFORM 16, Nantes, France.
[28] Dörr D, Joppich T, Schirmaier F, Mosthaf T, Kärger L, Henning F. Sensitivity of material properties on wrinkling behavior and fiber reorientation of thermoplastic ud-tape laminates during forming analyzed by finite element forming simulation. In: Proceedings ECCM17, Munich, Germany.
[29] Budiansky B, Sanders JL. On the 'best' first-order linear shell theory. Progress in applied mechanics (the Prager anniversary volume) 1963:129–40.
[30] Belytschko T, editor. Nonlinear finite elements for continua and structures. Chichester: Wiley; 2014. http://swbplus.bsz-bw.de/bsz399725997cov.htm.
[31] Hughes TJR, Winget J. Finite rotation effects in numerical integration of rate constitutive equations arising in large-deformation analysis. Numer Methods Eng 1980(15, 12):1862–7.
[32] Nelder JA, Mead R. A simplex method for function minimization. Comput J 1965(7):308–13.
[33] Macosko CW. Rheology: principles, measurements, and applications, advances in interfacial engineering series. New York: VCH; 1994.
[34] Peric D, Owen DR. Computational model for 3-d contact problems with friction based on penalty method 1992(35):1289–309.
[35] Spencer A. Deformation of fibre-reinforced materials. Oxford: Clarendon Press; 1972.
[36] Spencer A. Theory of fabric-reinforced viscous fluids. Compos Part A: Appl Sci Manuf 2000;31(12):1311–21. doi: http://dx.doi.org/10.1016/S1359-835X(00)00006-3.
[37] Kaliske M. A formulation of elasticity and viscoelasticity for fibre reinforced material at small and finite strains. Comput Methods Appl Mech Eng 2000;185(2–4):225–43. doi: http://dx.doi.org/10.1016/S0045-7825(99)00261-3.
[38] Rogers TG. Rheological characterization of anisotropic materials. Composites 1989(201):21–7.
[39] McGuinness G, ÓBrádaigh C. Development of rheological models for forming flows and picture-frame shear testing of fabric reinforced thermoplastic sheets. J Non-Newton Fluid Mech 1997;73(1–2):1–28. doi: http://dx.doi.org/10.1016/S0377-0257(97)00040-2.